THE JOURNAL OF PHYSICAL CHEMISTRY B LETTERS

2006, *110,* 7617−7620
Published on Web 03/30/2006

Elucidation of Codoping Effects on the Solubility Enhancement of Er^{3+} in SiO_2 Glass: Striking Difference between Al and P Codoping

Akira Saitoh,[†] Satoru Matsuishi,[†] Choi Se-Weon,[†] Junji Nishii,[‡] Masanori Oto,[§,||] Masahiro Hirano,[†,||] and Hideo Hosono*[,†,||]

Frontier Collaborative Research Center, Tokyo Institute of Technology, Nagatsuta, Midori-ku, Yokohama 226-8503, Japan, National Institute of Advanced Industrial Science and Technology, Midorigaoka, Ikeda, Osaka 563-8577, Japan, Showa Electric Wire and Cable, Minami-Hashimoto, Sagamihara 299-1133, Japan, and ERATO-SORST, Japan Science and Technology Agency, in Frontier Collaborative Research Center, Tokyo Institute of Technology, Nagatsuta, Midori-ku, Yokohama 226-8503, Japan

Received: February 2, 2006; In Final Form: March 21, 2006

The codoping effect mechanism of Al and P on the solubility enhancement of Er^{3+} ion in SiO_2 glass was clarified by electron spin−echo envelope modulation spectroscopy. It turned out that doped P ions preferentially coordinate to the Er^{3+} ion to form a "solvation shell structure", and the environment is similar to that in phosphate glass, while doped Al ions do not form such a selective solvation structure, taking octahedral coordination. This striking difference indicates that the primary roles of the P-doping and the Al-doping are attributed to "enthalpy of mixing" and to "entropy of mixing", respectively.

"Er^{3+}-doped fiber amplifier (EDFA)" using Er^{3+} ion activated SiO_2 glass fiber as an active media is a key component in the current fiber optics system because of its large optical gain over the spectral region of the 1.5-μm band, which is compatible with the long-haul optical fiber communication system.[1−5] However, at the early stage of the development, poor solubility of rare earth (RE) ions in SiO_2 glass, the solubility limit below ∼0.1 mol %, was a serious obstacle which made it difficult to attain sufficient gain for the optical amplification.[6−9] This difficulty has been overcome by doping of appropriate cations, typically Al^{3+} and P^{5+} ions, together with the Er^{3+} ion.[10−12] It is surprising that a kind of codoping works effectively for amorphous materials such as SiO_2 glass, because, in general, the addition of such a small amount of the second component gives no drastic changes in the properties of conventional glasses. Consequently, current EDFAs are based on Er^{3+}-activated SiO_2 glasses codoped with these cations.[3,4,6−8] However, despite intensive studies using X-ray absorption spectroscopy,[13−16] the microscopic mechanism for the codoping effect based on quantitative information about the local structure remains unclear to date, which restricts a further improvement of EDFA. Here, we report coordination structures of Er^{3+} ion in Al- and (Al + P)-codoped SiO_2 glasses through the analysis of pulsed-EPR electron spin−echo envelope modulation (ESEEM) spectra,[17,18] which reflects the intermediate-range structure (0.3−1 nm) around a paramagnetic center of the Er^{3+} ion ($4f^{11}$ configuration). We demonstrate that there is a striking difference in the formation of the solvation shell structure around the Er^{3+} ion between Al-codoped and (Al + P)-codoped SiO_2 glasses, suggesting the Al^{3+} and P^{5+} play totally different roles in the enhancement of the solubility of RE ions. Further, it is suggested that the random distribution of Al^{3+} yields the larger inhomogeneous broadening of the photoluminescence (PL) band of Er^{3+}, while the formation of the solvation shell structure by P^{5+} results in the narrower bandwidth.

TABLE 1: Analyzed Chemical Composition of the Samples

sample name	composition (mol%)			
ES	$0.02Er_2O_3$			$-$ $100SiO_2$
EAS	$0.1Er_2O_3$	$-$ $1.9Al_2O_3$		$-$ $98.0SiO_2$
EAPS	$0.1Er_2O_3$	$-$ $1.0Al_2O_3$	$-$ $0.9P_2O_5$	$-$ $98.0SiO_2$
EP	$0.1Er_2O_3$		$-$ $49.6P_2O_5$	$-$ $50.3CaO$

Nondoped (ES), Al-codoped (EAS), and (Al + P)-codoped (EAPS) SiO_2 glasses containing Er^{3+} ions were fabricated by a modified chemical vapor deposition process, in which Er^{3+} ions ($Er(C_5H_7O_2)_3 \cdot 2H_2O$) were doped by dipping the glass soots into the methanol solution. On the other hand, a phosphate glass (EP) was prepared by a conventional melt-quenching technique. The chemical compositions of the prepared glasses analyzed by an electron probe microanalyzer are listed in Table 1.

The two-pulsed (the $\pi/2 - \tau - \pi - \tau -$ echo sequence) field swept echo spectrum and the three-pulsed (the $\pi/2 - \tau - \pi/2 - T - \pi/2 - \tau -$ echo sequence) ESEEM spectrum were measured using an X-band pulsed-EPR spectrometer (E580, Bruker) attached to a dielectric resonator in a cryostat (Oxford Instruments). One of the critical conditions to obtain the spectrum with a high signal-to-noise ratio was measurement temperature: 4 K was insufficient, and thus, a spectrum at 3 K accumulated for ∼12 h was used for the present analysis. Calculation of ESEEM spectra was carried out by numerical diagonalization of the rotating spin Hamiltonian composed of

* Corresponding author: H. Hosono (hosono@msl.titech.ac.jp) Frontier Collaborative Research Center, Tokyo Institute of Technology, Nagatsuta, Midori-ku, Yokohama 226-8503, Japan; TEL +81-45-924-5359, FAX +81-45-924-5339.
† Tokyo Institute of Technology.
‡ National Institute of Advanced Industrial Science and Technology.
§ Showa Electric Wire and Cable.
|| Japan Science and Technology Agency.

10.1021/jp060702w CCC: $30.25

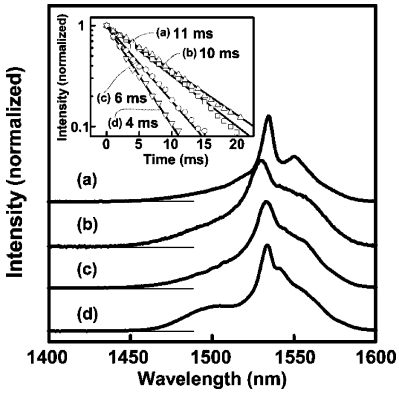

Figure 1. Fluorescence spectra of (a) ES, (b) EAS, (c) EAPS, and (d) EP at room temperature. Inset is fluorescence decay for each glass.

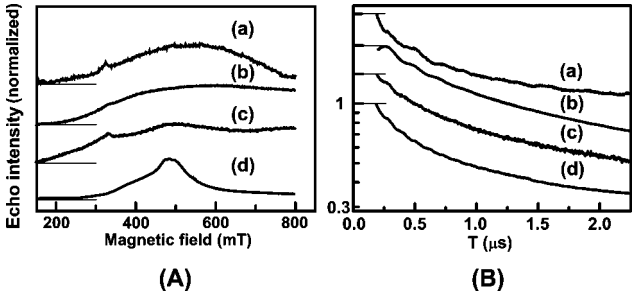

Figure 2. (A) Two-pulsed field-swept echo spectra for (a) ES, (c) EAPS, (d) EP, and (b) EAS, measured at 3 K. (B) Electron spin−echo decay curve of each sample in three-pulsed sequence. The measurement conditions are temperature = 3 K, static magnetic field = 500 mT, and τ = 172 ns for ES, EAPS, and EP, and 100 ns for (b).

a hyperfine, nuclear-Zeeman, and nuclear-quadrupole interactions. An algorithm reported in the previous paper[19] was employed for the simulation of the pattern.

The PL spectrum around 1.5 μm was measured with a monochromator (Spectra pro-2500i, Acton) equipped with a charged coupling device (CCD, Spec-m: 100BR, Princeton) under a 488-nm Ar^+ cw-laser light excitation. The decay of PL excited by the third harmonic of a Q-switched Nd:YAG laser (355 nm) was recorded using a CCD having an optical gate with an acquisition time of 1 ms.

Figure 1 shows PL spectra of (a) ES, (b) EAS, (c) EAPS, and (d) EP glasses along with the PL decay curves (inset). The spectrum of EAS is significantly different from the others; the apparent main peak is shifted to a shorter wavelength, and the bandwidth is largest among the samples. A weak subpeak is seen at the longer-wavelength side of the main peak in ES, and it becomes broader, giving a shoulder at the position of the main peak in the other glasses. These observations suggest that the codoping of Al^{3+} results in the more enhanced broadening of the PL bands compared to the nondoping (ES), the P-codoping (EAPS), and the phosphate glasses (EP). The PL lifetimes of EAPS and EP exhibit nearly the same value of ~5 ms, which is approximately half of those of ES and EAS, indicating the P-codoping makes the PL lifetime shorter.

Figure 2A shows the field-swept echo spectra. Very broad and featureless absorptions peaking at ~500 mT due to paramagnetic Er^{3+} are observed for each sample. Figure 2B shows electron spin−echo decay curves of the glasses at a static magnetic field of 500 mT, where the decay is caused by the spin−lattice relaxation. Weak but distinct modulation due to a magnetic nucleus is observed to superpose on each decay curve.

Observed and simulated ESEEM spectra of the Al-codoped (EAS) are shown in Figure 3A, and the (Al + P)-codoped

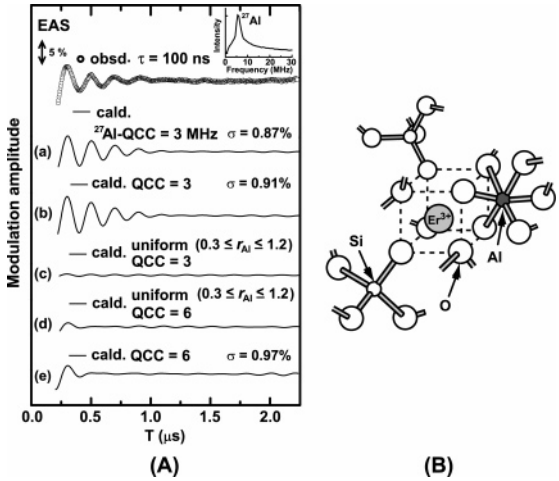

Figure 3. (A) Observed (circles) and calculated (solid) ESEEM spectra of EAS. Distance (r), number (N), and quadrupolar coupling constant (QCC) of ^{27}Al nucleus, which were used for the calculation, are shown for each calculated curve. The best-fit curve is shown in (a), where (r_{Al}, N_{Al}) = (0.30 nm, 0.3) and QCC = 3 MHz. (b) Pattern calculated for the simple mixture of an Al (octahedral site at r = 0.3 nm) bearing coordination (30%) and Al-free coordination (70%). Tetrahedral Al^{3+} (QCC = 6 MHz) did not fit the observed curve as shown in (e). The patterns (c) and (d) were obtained for the uniform distribution model in the range 0.3−1.2 nm from Er^{3+}. (B) Coordination structure models for Er^{3+} in EAS glass deduced from the best-fit curve. Only cations and anions relevant to the model are described for simplicity. The standard deviation σ for each fitting is shown.

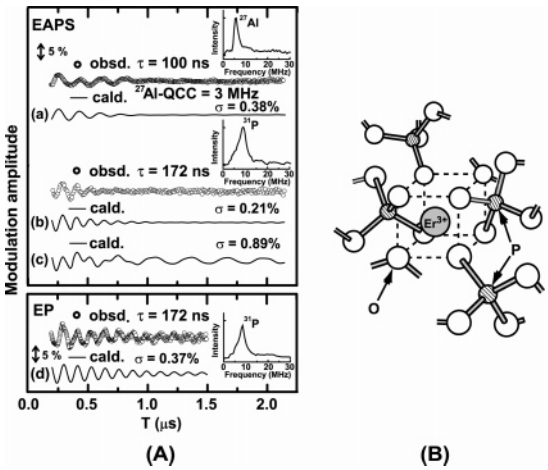

Figure 4. (A) Observed (circles) and calculated (lines) ESEEM spectra of EAPS and EP. Insets are FT-ESEEM. Curves (a) and (b) are fitted to the modulations due to ^{27}Al and ^{31}P nuclei in EAPS, respectively. Curve (c) is a calculated pattern for $AlPO_4$-like structure, where P^{5+} coordination is the same as that for curve (b), and (r_{Al}, N_{Al}) = (0.32 nm, 0.2) and QCC = 3 MHz. Curve (d) the best fit for EP, where (r_P, N_P) = (0.30 nm, 4) and (0.40 nm, 4). (B) Phosphorus-solvation shell structure around an Er^{3+} in EAPS. Octahedrally coordinated Al^{3+} ion, which is located at the second nearest-neighbor site with an occupation probability of 0.2, is eliminated in part B. The standard deviation σ for each fitting is shown.

(EAPS) glasses and those of phosphate glass (EP) are shown in Figure 4A.[20] Fourier transformed (FT) ESEEM in the insets of Figures 3A and 4A revealed that the magnetic nucleus responsible for the modulation is ^{27}Al ($I = {}^5/_2$, natural abundance = 100%) for EAS, ^{31}P ($I = {}^1/_2$, 100%) and ^{27}Al for EAPS, and ^{31}P for EP.

We calculated ESEEM patterns of EAS under a condition that only ^{27}Al gives the modulation, and the contribution from ^{29}Si ($I = {}^1/_2$, 4.67%) is negligible as revealed from the FT-

ESEEM in the inset of Figure 3A. First, the simulation was performed for the uniform distribution of Al^{3+} around an Er^{3+} in the glass matrix treated as a uniform media. Thus, the number of Al^{3+} ions continuously increases proportionally to the cubic distance from the Er^{3+} ion. In addition, we calculated the modulations for two values of ^{27}Al quadrupolar coupling constant (QCC = 3 and 6 MHz), because there are two possible coordination of Al^{3+} ion in oxide glasses, an octahedral AlO_6 coordination in which an Al^{3+} ion works as a network modifier and a tetrahedral AlO_4 in which an Al^{3+} ion serves as a network former; and further ^{27}Al NMR studies revealed that the QCC values for these two types of the coordination are distinctly different: ~3 MHz for the AlO_6 and ~6 MHz for the AlO_4.[21,22] The simulated modulation intensities for the two possible QCC values are too small to be fitted to the observed pattern as shown in curves b and c in Figure 3, indicating that the simple uniform distribution model is obviously invalid for EAS. Then, the modulation patterns were calculated by changing the distance (r_{Al}) between Er^{3+} and Al^{3+} and the number of ^{27}Al nucleus (N_{Al}) independently. The calculations were also performed for the QCC values of 3 and 6 MHz. As results, we obtained an excellent fitting when we took $r_{Al} = 0.30$ nm, $N_{Al} = 0.3$, and QCC = 3 MHz as shown in curve a of Figure 3. If we took the QCC value to be 6 MHz, keeping $r_{Al} = 0.30$ nm and $N_{Al} = 0.3$, the modulation amplitude (curve e) becomes much less than that in the observed pattern, indicating that the Al^{3+} attaching to the Er^{3+} takes an octahedral coordination, not tetrahedral coordination. The r_{Al} value of 0.30 nm may give rise to a structure in which an Al^{3+} ion coordinates to an Er^{3+} ion through two edge-sharing oxygen ions. N_{Al} within $r = 0.6$ nm expected from the codoped Al^{3+} ion concentration under the homogeneously distribution is 0.2, which is in reasonably good agreement with the obtained value of 0.3 (N_{Al}). Here, note that the number (0.3) of Al^{3+} obtained through simulation is lower than 1. This value means that the coordination sphere of Er^{3+} is a mixture of an Al^{3+} ion-bearing coordination (30%) and Al-free coordination (70%). Calculated curves in Figure 3a,b were almost the same fitting for the observed pattern. From these analyses, we obtain a most plausible coordination structure around the Er^{3+} ion in EAS as shown in Figure 3B, where the octahedrally coordinated Al^{3+} ions are not preferentially coordinated to the Er^{3+} ion.

Figure 4A shows observed and calculated ESEEM spectra of the (Al+ P)-codoped SiO_2 (EAPS) and the phosphate glass (EP) samples. Insets are the FT-ESEEM spectra for the EAPS and EP, showing ^{31}P contributes to ESEEM of EP and both ^{31}P and ^{27}Al contribute to that of EAPS. The magnetic nucleus controlling the modulation can be switched from ^{27}Al to ^{31}P by tuning the pulse interval τ from 100 to 172 ns as shown in the inset. By utilizing this technique, we can determine the coordination structures associated with Al^{3+} and P^{5+} ions in EAPS separately. The modulation pattern calculated for the simple uniform distributions of both the Al^{3+} ions (~1 mol % Al_2O_3) and P^{5+} (~1 mol % P_2O_5) was rather deviated from the observed pattern. As for the coordination of the doped Al^{3+} ion in the EAPS, the best fit was attained by assuming (r_{Al}, N_{Al}) = (0.32 nm, 0.2) and the ^{27}Al-QCC = 3 MHz. Here, we checked validity of this fitting result of fractal number of Al^{3+} ($N_{Al} = 0.2$) by calculation as is the case of EAS sample. Namely, the pattern calculated for a mixture model of 20% (r_{Al}, N_{Al}) = (0.32 nm, 1) and 80% (0.32 nm, 0) was pretty close to that for the (r_{Al}, N_{Al}) = (0.32 nm, 0.2). This result indicates that an octahedrally coordinated Al^{3+} ion participates in the second neighbor of the Er^{3+} ion with an occupation probability of 0.2, and no preferential coordination of the Al^{3+} ion to the Er^{3+} ion is seen as in the case of the EAS. On the other hand, the best-fit pattern to the observed spectrum due to P^{5+} ions was obtained by assuming that four P^{5+} ions are involved in the coordination sphere of the Er^{3+}; two of them are positioned at 0.30 nm, and the other two are at 0.40 nm as shown in Figure 4Ab. This coordination structure was very similar to that in the (Ce^{3+} + P)-codoped SiO_2 glass.[23] Since P^{5+} ions tetrahedrally coordinate to oxygen ions, $r_P = 0.30$ nm corresponds to a structure in which a P^{5+} ion bonds with an Er^{3+} ion through two edge-sharing oxygen ions, while $r_P = 0.40$ nm provides a structure in which a P^{5+} ion coordinates to an Er^{3+} ion through a nonbridging oxygen ion in $P-O^-$ group. The total number of P^{5+} ions in the coordination sphere is 4, which is larger by a factor of 10 than that expected from the uniform distribution of P^{5+} ions in the glass (0.4 within $r = 0.6$ nm), indicating that P^{5+} ions form a distinct "solvation shell structure" as shown in Figure 4B. Further, a distinct disagreement of the calculated curve for the $AlPO_4$-like structure, Figure 4Ac, ruled out a possibility for the direct bonding formation of Al^{3+} and P^{5+} via a bridging oxygen ion. Consequently, the local environment of Er^{3+} ions in EAPS is provided by a simple superposition of those formed by the Al and P dopings.

In the EP sample, the best-fit curve, Figure 4Ad, was obtained for a coordination structure in which four P^{5+} ions are positioned at r_P = both 0.30 and 0.40 nm, which is similar to that of the EAPS except for the value of N_P, suggesting that two types of $P-O$ bond coordination to an Er^{3+}, in corner-sharing and edge-sharing manners, commonly exist in the P-codoped SiO_2 glass and the phosphate glass. The same coordination structure was obtained for Ce^{3+}-activated SiO_2 glass codoped with P,[23] suggesting the common coordination structure for RE^{3+} ion in P-codoped SiO_2 glass.

It has been believed to date that the roles of Al^{3+} and P^{5+} are essentially the same, and the solubility of Er^{3+} ion is enhanced by the preferential coordination to the activated ion in both cases. However, the present study has revealed that there is a striking difference in the coordination structure of an Er^{3+} ion between the EAS and the EAPS glasses: Doped P^{5+} ions preferentially coordinate to the Er^{3+} ion, whereas doped Al^{3+} ions do not show such a tendency. Our findings indicate that the roles of Al^{3+} and P^{5+} ions in the solubility enhancement differ distinctly from each other. In general, the codoped glass phase is stabilized due to a decrease in "enthalpy" or an increase in "entropy" relative to that of the corresponding segregated phase. Therefore, we consider that the enthalpy of mixing is dominant for the P-doping, because the formation of the solvation shell structure reduces enthalpy. On the other hand, the Al-doping enhances the solubility by the factor of the entropy of mixing, because octahedrally coordinated cation sites were increased by the Al-doping, at which an Er^{3+} ion can substitute.

Finally, observed PL properties are discussed on the basis of the elucidated coordination structures. The PL spectra and the radiative lifetimes of Er^{3+} ion are strongly influenced by its ligand field, which is dominantly governed by type and geometrical structure of the nearest-neighbor oxygen ions. For instance, the nearest-neighbor oxygen ions in the EAPS are composed of four edge-sharing (O_E), two corner-sharing (O_C), and two silica network forming types (O_N), as shown in Figure 4B, and there is a fluctuation in terms of an occupation number of each type of oxygen ion (N_C). The similarity of PLs of the EAPS to that of the EP is understood because Er^{3+} ions in both glasses have similar nearest-neighbor coordination structures regulated by the phosphate anions.[14,16] On the other hand, the

nearest neighbor in the EAS is composed of the O_N and a pair of O_E attaching to an octahedral Al^{3+} as shown in Figure 3B, in which the O_E distributes in such way that the occupation probability of an octahedral Al^{3+} is ~0.2, i.e., an Er^{3+} with Al^{3+}-free and an Er^{3+} with an Al^{3+} coexist. Thus, a noticeable variation in the N_C occurs, which, together with the geometrical disorder inherent to SiO_2 glass phase, leads to a large distribution in the ligand field over Er^{3+} sites. Such large variation of the crystal field on Er^{3+} leads to a marked broad feature of the PL spectrum of the EAS, which is a major advantage for wideband amplification in practical EDFA applications.[6,7] Thus, it may be concluded that the larger inhomogeneous broadening of PL in the Al-codoped SiO_2 glasses than in the (Al + P)-codoped SiO_2 glasses is well-correlated with the difference in the elucidated coordination structures.

The present study has deduced the solvation shell models in codoped SiO_2 glasses, which provide not only a microscopic image on the critical role of codopants in SiO_2 glass but a guiding principle for choosing effective codopants for the improvement of the solubility and consequently PL performance of RE ion.

References and Notes

(1) Koester, C. J.; Snitzer, E. *Appl. Opt.* **1964**, *3*, 1182.
(2) Snitzer, E.; Woodcock, R. *Appl. Phys. Lett.* **1965**, *6*, 45.
(3) Ainslie, B. *IEEE J. Lightwave Technol.* **1991**, *9*, 220.
(4) Miniscalno, W. J. *IEEE J. Lightwave Technol.* **1991**, *9*, 234.
(5) Desurvire, E. *Phys. Today* **1994**, *47*, 20.
(6) Yamada, M.; Shimizu, M.; Ohishi, Y.; Horiguchi, M.; Sudo, S.; Shimizu, A. *Electron. Lett.* **1994**, *30*, 1762.
(7) De Barros, M. R. X.; Nykolak, G.; DiGiovanni, D. J.; Bruce, A.; Grodkiewicz, W. H.; Becker, P. C. *IEEE Photon. Technol. Lett.* **1996**, *8*, 761.
(8) Hwang, B.-C.; Jiang, S.; Luo, T.; Seneschal, K.; Sorbello, G.; Morrell, M.; Smektala, F.; Honkanen, S.; Lucas, J.; Peyghambarian, N. *IEEE Photon. Technol. Lett.* **2001**, *13*, 197.
(9) Seneschal, K.; Smektala, F.; Bureau, B.; Le Floch, M.; Jiang, S.; Luo, T.; Lucas, J.; Peyghambarian, N. *Mater. Res. Bull.* **2005**, *40*, 1433.
(10) Arai, K.; Namikawa, H.; Kumata, K.; Honda, T.; Ishii, Y.; Handa, T. *J. Appl. Phys.* **1986**, *59*, 3430.
(11) Arai, K.; Namikawa, H.; Ishii, Y.; Imai, H.; Hosono, H.; Abe, Y. *J. Non-Cryst. Solids* **1987**, *95* & *96*, 609.
(12) Hosono, H.; Zuhr, R. A. *J. Non-Cryst. Solids* **1994**, *178*, 160.
(13) Okumura, H.; Kakuta, N.; Ueno, A.; Morino, R.; Mizushita, T.; Udagawa, Y.; Namikawa, H. *Chem. Lett.* **1989**, 829.
(14) Peters, P. M.; Houde-Walter, S. N. *J. Non-Cryst. Solids* **1998**, *239*, 162.
(15) Sen, S. *J. Non-Cryst. Solids* **2000**, *261*, 226.
(16) Karabulut, M.; Marasinghe, G. K., Metwalli, E.; Wittenauer, A. K.; Brow, R. K.; Booth, C. H.; Shuh, D. K. *Phys. Rev. B* **2002**, *65*, 1042061.
(17) (a) Rowan, L. G.; Hahn, E. L.; Mims, W. B. *Phys. Rev.* **1965**, *137*, A61. (b) Mims, W. B. *Phys. Rev. B* **1972**, *5*, 2409.
(18) (Books on ESEEM) (a) Schweiger, A.; Jeschke, G. *Principles of pulse electron paramagnetic resonance*; Oxford University Press: Oxford, 2001. (b) Dikanov, S. A.; Tsvetkov, Y. D. *Electron Spin−Echo Envelope Modulation (ESEEM) Spectroscopy*; CRC Press: Boca Raton, 1992.
(19) (a) Dikanov, S. A.; Shubin, A. A.; Parmon, V. N. *J. Magn. Reson.* **1981**, *42*, 474. (b) Shubin, A. A.; Dikanov, S. A. *J. Magn. Reson.* **1983**, *52*, 1. (c) Matsuishi, S.; Hayashi, K.; Hirano, M.; Tanaka, I.; Hosono, H. *J. Phys. Chem. B* **2004**, *108*, 18557.
(20) The intensity of ESEEM for EAS is similar to that for EAPS. However, this similarity does not imply the similar coordination number of Al and P. Since the ESEEM intensity is proportional to $I(I + 1)$ of interacting nucleus (I = nuclear spin), the difference between ^{31}P ($I = {}^1/_2$) and ^{27}Al ($^5/_2$) gives a large intensity difference.
(21) Baltisberger, J. H.; Xu, Z.; Stebbins, J. F.; Wang, S. H.; Pines, A. *J. Am. Chem. Soc.* **1996**, *118*, 7209.
(22) Schaller, T.; Stebbins, J. F. *J. Phys. Chem. B* **1998**, *102*, 10690.
(23) Saitoh, A.; Matsuishi, S.; Oto, M.; Miura, T.; Hirano, M.; Hosono, H. *Phys. Rev. B* **2005**, *72*, 2121011.